ARCHITECTURAL ROBOTS



# Toward site-specific and self-sufficient robotic fabrication on architectural scales

**Steven J. Keating, Julian C. Leland, Levi Cai, Neri Oxman***

**Contemporary construction techniques are slow, labor-intensive, dangerous, expensive, and constrained to primarily rectilinear forms, often resulting in homogenous structures built using materials sourced from centralized factories. To begin to address these issues, we present the Digital Construction Platform (DCP), an automated construction system capable of customized on-site fabrication of architectural-scale structures using real-time environmental data for process control. The system consists of a compound arm system composed of hydraulic and electric robotic arms carried on a tracked mobile platform. An additive manufacturing technique for constructing insulated formwork with gradient properties from dynamic mixing was developed and implemented with the DCP. As a case study, a 14.6-m-diameter, 3.7-m-tall open dome formwork structure was successfully additively manufactured on site with a fabrication time under 13.5 hours. The DCP system was characterized and evaluated in comparison with traditional construction techniques and existing large-scale digital construction research projects. Benefits in safety, quality, customization, speed, cost, and functionality were identified and reported upon. Early exploratory steps toward self-sufficiency—including photovoltaic charging and the sourcing and use of local materials—are discussed along with proposed future applications for autonomous construction.**

## INTRODUCTION

Construction shapes our modern world. With global annual output in excess of $8.5 trillion (*1*), construction is an integral part of the global economy's backbone, yet it relies on traditional fabrication technologies that are dangerous, slow, and energy-intensive. Common labor-intensive processes—including bricklaying, wood framing, and concrete casting—have, for decades of design construction, put workers at risk. The International Labour Organization estimated in 2005 that more than 50,000 people die globally in the construction industry per year, accounting for 17% of workplace accident fatalities (*2*).

To improve safety, speed, and quality and to facilitate complex integrative fabrication operations, other manufacturing sectors—such as automotive and consumer electronics—have adopted the use of automated fabrication. Automated construction systems promise to yield similar benefits to the construction industry and, moreover, make newer digital fabrication techniques available at large scale. In combination with layer-based and freeform additive manufacturing techniques, automated construction systems could produce geometries that would be economically, if not physically, impossible to realize with conventional construction techniques. Structures produced by automated construction systems could be adapted on the fly to site-specific environmental conditions and constraints, using data collected in real time during fabrication. This capacity for data collection could also support more direct, detailed quantification of the building process, generating valuable data sets and describing a structure's construction in high detail. Last, automated construction systems that could operate autonomously would find ideal applications performing construction tasks in inhospitable (such as after natural disasters) or extreme (such as Arctic or even extraterrestrial) environments.

Thomas Edison made the first substantial attempt at construction automation with his prototype single-pour housing mold in the early 1900s, although the project was a failure and resulted in the bankruptcy of his concrete company (*3*). Industry and academic researchers began to explore introducing automation to construction tasks beginning in the early 1980s, particularly in Germany and Japan (*4*, *5*). The past three decades have seen the field of automated construction grow substantially, which has led to the creation of a wide range of system/process combinations, including bricklaying robotic arms (*6*–*8*), filament winding of structural composite parts (*9*), and gantry systems for three-dimensional (3D) printing of concrete (*10*–*12*). More recent work has begun to explore the use of multiple small, mobile agents to complete fabrication tasks using lightweight materials (*13*, *14*) and to develop systems that can reposition and relocalize to expand their work volume (*15*).

Although there are diverse research approaches to automated construction (*16*), there is no consensus on the best approach, and none of the systems being developed have yet entered industry in a substantial manner. As a means for comparing existing systems and determining an optimal path for the development of future automated construction systems, we have identified the following major debates in the field.

### Where to build—In a factory, on site, or a combination

The design of buildings is strongly linked to the environmental conditions of their sites. Ground stability, the presence of extreme winds, or other environmental and social factors will determine the construction techniques and materials that are necessary to build safe, usable structures. These, in turn, dictate the capabilities required of the construction system itself.

The first point of classification is thus systems that manufacture prefabricated components in an off-site factory environment, systems that perform fabrication tasks directly on site, and systems that perform a combination of both. Creating prefabricated structures in a factory offers some substantial benefits, such as ensuring a highly controlled environment for fabrication, enabling machines to be set up permanently for mass production, and eliminating costs associated with transporting fabrication tools (*17*). Prefabrication has been widely used in the construction industry, with examples ranging from precast concrete blocks to radio tower truss sections. As an example of prefabrication in automated construction work, the WinSun Company has successfully built a series of structures in China using prefabricated, 3D-printed concrete components (*18*).

Mediated Matter Group, MIT Media Lab, Massachusetts Institute of Technology, Cambridge, MA 02139, USA.
*Corresponding author. Email: neri@mit.edu

However, prefabrication is limited by a range of costs and constraints associated with transportation and assembly and by poor customizability of structures, which can pose particular challenges when information about build sites is limited or inaccurate. Raw materials need to be transported to a centralized factory, processed, and then shipped to the site. For large structures, such as buildings and civil infrastructure, transportation can be constraining due to volumetric limitations and the absence of roads. For structures being built in remote or extreme locations, sufficient information about the environment can be challenging to obtain and hence affect the ability to plan a structure.

Autonomous on-site construction can offer improved worker safety, improved process control and quantification, and last-minute adaptability to local conditions. Although prefabrication is a convenient stepping stone for the field, we believe that on-site fabrication will rapidly displace it as automated construction systems take a greater role on the construction site.

## How to build—Materials and processes

The fabrication processes implemented by different automated construction systems are quite diverse and tightly coupled with the environmental requirements of the structures, but most can be generally grouped into (i) material extrusion processes and (ii) assembly processes. We are generally process-agnostic, recognizing that a wide range of materials and fabrication techniques are required to construct a complete structure, and we instead emphasize the importance of automated construction systems that can implement multiple fabrication techniques. However, material extrusion processes offer a number of capabilities that assembly-based processes cannot, including fabrication of arbitrarily complex forms without additional material/time cost and the ability to create continuous gradients in printed material, which could impart valuable functionality [such as directly printed earthquake dampers (*19*)] into built structures.

## Static or mobile platform

Historically, most of the automated construction systems explored have been functionally static, either because they are too large and unwieldy to safely move even if they operate on site (*20*, *21*) or because they are intended to operate as prefabrication systems in factory conditions, as with most gantry-style systems. Static systems generally benefit from simpler construction, design, and operation.

The most common static platforms are gantry-style systems, which generally have 3 degrees of freedom (DOFs) and are unable to handle complex geometries and overhangs. Even small arms mounted on gantry systems (*22*) rapidly encounter issues with collision with the structure when attempting to fabricate overhang-like structures. Static systems also require assistance from either a human-operated device or another autonomous system for transportation to and set up at a work site (*21*).

More recent work has begun to explore mobile platforms for construction. Mobility rapidly becomes imperative as researchers seek to develop systems with much larger build volumes, to enable fully autonomous on-site fabrication, and to effectively deploy automated construction systems in swarm configurations.

Mobile systems can be classified as terrestrial or aerial. Terrestrial systems remain on the ground and primarily increase lateral work volumes (*23*, *24*). Aerial drone-based systems (*13*) provide theoretically unlimited work volume across all dimensions and tremendous operational flexibility. However, they are typically restricted to assembly tasks (*13*, *25*) and also suffer from major constraints associated with flight, such as high energy costs, limited load capacity, fabrication time limitations due to battery/fuel consumption, complex control requirements, and substantial hazard associated with system failure. Environmental factors, such as wind, rain, and wildlife, are also important challenges. Thus, terrestrial systems can provide increased work volumes and swarm capabilities without incurring heavy costs on complexity of the system itself.

## Evaluating the ideal system form factor

Automated construction systems have been implemented using a wide range of kinematic structures, but most can be sorted into one of three major categories: gantries (*26*), aerial drones, and robotic arms. Each category has different benefits, disadvantages, suitability for varying applications, and challenges for the future.

A conventional gantry system with Cartesian kinematics is relatively simple to control and is capable of carrying heavy loads, as demonstrated by existing large-scale fabrication projects (*10*). However, gantry systems are constrained to a work volume with limited operational flexibility, which is especially important for producing complex overhang forms and working on existing structures. In addition, gantry systems require longer setup and takedown times, need a large space for installation due to a substantial physical footprint, and cannot easily scale to accommodate structures larger than the work volume of the gantry.

Arm-based systems offer a compromise between complexity and robustness relative to gantry and aerial architectures. For automated operation, arm-based robotic systems can be more complicated to control and more sensitive to disturbances than conventional Cartesian gantries but substantially less complex than aerial-based systems. Load capacities of robotic arm systems are also generally lower than gantry systems but substantially higher than aerial drones.

Arm-based systems also provide substantial benefits when used for construction tasks. Arm-based systems offer high kinematic flexibility to enable fabrication of complex structures, such as doubly curved forms that require control of the orientation of the end effector. This increased dexterity can also allow arms to perform more sophisticated operations and adapt to varying construction environments. Arm systems also have a very large ratio of physical reach to platform footprint, enabling simpler access to complex sites and allowing extremely large work volumes.

Arm-based systems naturally complement mobile bases. In addition to increased work volumes, they are able to relocate to print in otherwise self-colliding configurations. For instance, many arm robots are unable to reach near their own body due to kinematic constraints, but this is nullified if they are able to move away entirely. There has been substantial research conducted exploring problems of mobile manipulation using small-scale industrial and research arms, which arm-based automated construction systems can easily leverage.

Last, the substantial use of nonautomated arm systems in the traditional construction industry is an important factor. There is an existing engineering and manufacturing ecosystem that can support the development of arm-based vehicles, including possibilities of converting existing machines to autonomous systems. Furthermore, arm-based systems can leverage decades of research into conventional serial-link manipulator robots to expand their capabilities.

On the basis of these methodological questions, an arm-based automated construction system was designed, built, and tested. The system, called the Digital Construction Platform (DCP), consists of combined hydraulic and electric robotic arms in a micro-macro manipulator configuration, mounted on a tracked mobile base. The prototype system described here is the second iteration of the DCP system and

is based on previous research in our group that began in early 2011 (*27*, *28*). We describe the DCP's design philosophy and construction and report basic performance metrics for the system.

To evaluate the platform, a case study project was conducted using the DCP to fabricate a 14.6-m-diameter, 3.7-m-tall hemispherical open dome. The dome was constructed using a 3D printing process we call print-in-place (PiP) fabrication (*28*), which uses two-part spray polyurethane foam to additively fabricate formworks for cast concrete structures, rather than fabricating directly using a structural material.

We then present our work in the context of other contemporary automated construction systems and discuss how the methodological questions described here correlate with system performance. Last, we discuss initial explorations of energy sourcing, local material gathering, and mobility toward the goal of fully autonomous, self-sufficient, on-site construction.

## RESULTS

### The Digital Construction Platform

The DCP design concept is based around a mobile compound robotic arm system composed of a large, 4-DOF hydraulic arm with a smaller, 6-DOF electric arm attached at its endpoint (Fig. 1). Akin to the biological model of a human shoulder and hand, this compound system uses the large arm for gross positioning and the small arm for fine positioning and oscillation compensation. Compound arm systems like this are commonly known as micro-macro manipulators. They were first described by Sharon *et al.* (*29*) and have found application in space robotics, construction, hazardous material management, and more (*30*–*32*). The prototype DCP is composed of a 2015 Altec AT40GW aerial lift system, with a KUKA AGILUS KR 10 R1100 sixx WP electric robotic arm mounted at the aerial lift's endpoint. The electric arm was selected on the basis of its high joint accelerations, fast real-time control interface, low weight, and IP67 rating. When integrated, the DCP prototype has a radial reach of more than 10 m and a load capacity of 158 kg lifted/10 kg manipulated. The DCP is designed to be material- and process-independent, allowing for fabrication in additive, subtractive, and formative modes with a wide range of materials.

The measured characteristics and specifications of the DCP are detailed in Table 1. A short overview video of the DCP system is included in the Supplementary Materials (movie S1).

#### *Control of the compound arm system*

In traditional fused deposition printing of plastics, the material feed rate, deposition pattern, and layer-by-layer adhesion properties of the material determine the necessary position and velocity control schemes of the printer head. Specifically, printers must accurately track Cartesian space (as opposed to joint space), positions, and velocities to maintain uniform material deposition throughout the print. Deviations in the trajectory, vibrations, and other potential sources of error can drastically affect the outcome of the final print and adversely affect layer-to-layer adhesion. These same principles are generally true when fabricating objects using two-part polyurethane spray foams, as in PiP fabrication, and hence, deriving appropriate controllers to simultaneously track position and velocity references is crucial for successful prints.

There are several overall control modes for the compound arm system of the DCP that can be used interchangeably for different tasks or even different segments of a single print. The first mode allows for independent control of the hydraulic boom arm and the KUKA arm such that only one system is moving during a given toolpath segment. A second operational mode is coupled motion of the hydraulic boom arm with the KUKA. Within this mode, there can be many submodes, such as using the KUKA for only vibration dampening or as a method for following toolpaths and tasks that require higher resolution. In the work described here, the first mode was used during larger-scale prints; the latter modes were initially explored and are currently under further development.

With a feedforward velocity and position proportional-integral-derivative (PID) controller on each joint of the hydraulic arm, the end effector of the hydraulic section of the DCP can track quintic spline toolpaths at Cartesian velocities between 50 and 300 mm/s with a feedback loop operating at roughly 100 Hz. When combined with real-time control of foam spray rate, this allows for a wide range of foam deposition widths, as discussed in "Basic print testing" below. One potential issue faced by arm-based systems is that normal accelerations in Cartesian space may correspond to fairly high or low joint-space accelerations, depending on system pose. We found that our system is generally able to maintain the Cartesian velocities listed without incurring substantial noise. However, if a different extrusion material or fabrication technique that required deviation from this speed range were to be used, then modifications to the controller and sensor architecture might be necessary.

Independent control of the hydraulic aerial lift unit was characterized with an external laser optical tracking system (Leica Absolute Tracker AT901). The pose repeatability of the AT40GW was characterized in accordance with the International Organization for Standardization (ISO) 9283-1998 industrial robot performance standard (*33*), using a five-point trajectory in a volume measuring 1.5 m by 2 m by 1.5 m. The test trajectory was executed 30 times, as specified in the standard. Results from this test are seen in Fig. 2B, and fully detailed in text S1. We also report the mean of pose repeatability error and standard deviation measured over all five points in the trajectory in Table 1. Note that—to capture the pose repeatability of the AT40GW on its own—the KUKA robotic arm was not active during this test.

To inspect the results of the ISO 9283-1998 tests, a second repeatability test of movements between two randomly chosen points was conducted. Points were selected that necessitated the movement of all of the hydraulic aerial lift unit's joints. DCP movements to each point occurred 35 times, with a delay time of 30 s after stopping at each point. From the 70 endpoint measurements of the AT40GW, a mean average difference of 9.03 mm with an SD of 4.20 mm was found. These results are within the range of results from the ISO repeatability test.

Although these tests do not directly characterize the DCP's repeatability when following a trajectory, they provide a useful starting point for understanding the system's performance, and further testing in fabrication applications has demonstrated that the DCP's performance is sufficient to implement additive fabrication processes successfully. In the case of PiP fabrication particularly, the large deposition width (which can range from 3 to 20 cm) and the robustness of the foam to imperfections in target spray surface yield good results when implemented with the DCP.

Long-exposure photography was used to create a visual record of the DCP's kinematics and capabilities. Figure 3 highlights the reach of both arm systems. By simultaneously executing programs using both arms, more complex tool paths are possible, as seen in Fig. 3 (A and B).

#### *Real-time environmental data*

To adapt to environmental conditions and compensate for oscillations of the AT40GW, real-time sensor feedback can be used to drive the KUKA arm, enabling it to stabilize the DCP's endpoint. With the laser sensor mounted on the KUKA wrist, variations in ground height were measured and compensated for by the KUKA as the AT40GW moved. This process enabled the DCP's endpoint to maintain a constant

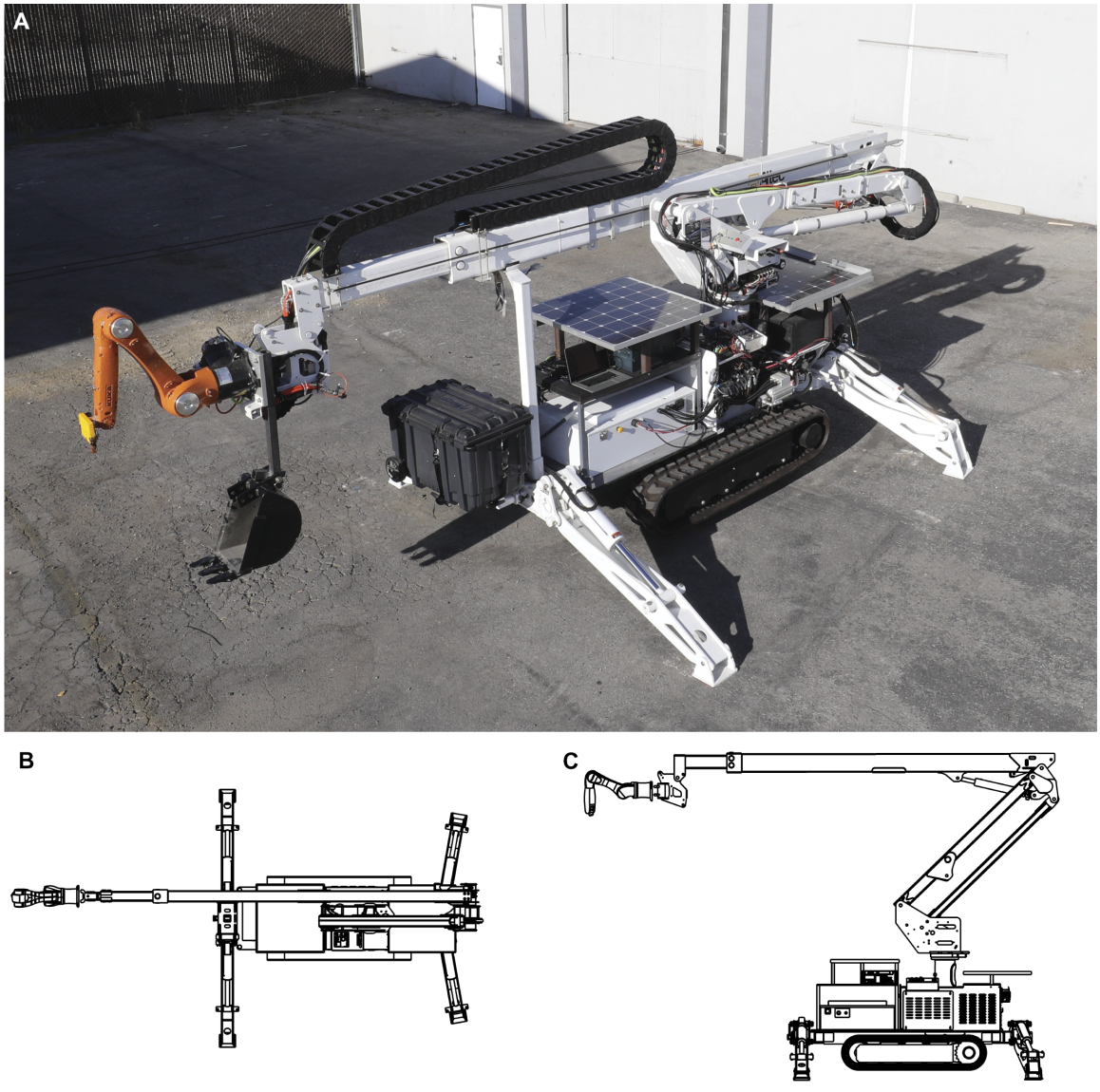


**Fig. 1. The DCP.** (**A**) Full system with excavator attachment. (**B**) CAD rendering, top view. (**C**) CAD rendering, side view.

aboveground height based on environmental feedback, as seen in movie S1 and fig. S1. This system was demonstrated to be robust for a range of ground surface conditions and at high endpoint translation rates. To quantify the results, the AT40GW was programmed to execute a series of vertical movements, whereas the KUKA arm attempted to compensate for these motions and maintain a constant endpoint position using real-time feedback from the laser sensor. The endpoint position of the KUKA was externally measured with a Leica AT901 laser tracker system. The results comparing compensated with uncompensated movements are shown in fig. S2.

***Platform mobility***

To maximize build volume and enable full autonomy, the DCP was equipped with a track-based mobile platform. The DCP's mobile base can be used in two distinct strategies. One strategy is to print while driving. This can provide much larger continuous work volumes but requires full-body motion planning to account for additional DOF. The second strategy, which is the focus of this and similar work (*15*, *24*), is to print from a stationary position and then move to another position only when needed.

The tracks are capable of expanding laterally to increase stability and contracting to fit through standard doorways. The tracked unit is powered by a hydraulic motor and controlled by proportional solenoid valves. An interface connection was added to the handheld drive controller on the AT40GW, providing digital control of the treads to enable automated driving. As with similar construction vehicles, the DCP has hydraulic outriggers that are usually deployed during prints to assist with stability. A connection to the valves controlling the extension of the stabilizer outriggers was added to enable automated setup on site.

Programmable control of DCP mobility and outrigger setup was demonstrated with variable drive speeds and platform rotation using open-loop independent tank tread control. As a demonstration, a DCP program enabled the unit to drive autonomously out of its garage, turn and park at a fixed location, extend its side outriggers, and write the word "hi" on a whiteboard using a combination of both hydraulic

**Table 1. DCP system performance specifications.**

| | | | | | |
|---|---|---|---|---|---|
| Maximum radial reach (m) | 10.1 | | | | |
| Maximum vertical reach (m) | 14.1 | | | | |
| Maximum printable volume ($m^3$) | 2,786 | | | | |
| Mobile | Yes | | | | |
| Type of mobility | Tracks | | | | |
| System weight (kg) | 3,700 | | | | |
| Photovoltaic charging | Yes | | | | |
| Power source | Battery/plug-in/diesel | | | | |
| System cost (USD) | 244,500 | | | | |
| Maximum driving speed (m/s) | 0.550 | | | | |
| Minimum driving speed (m/s) | 0.006 | | | | |
| Lift capacity at endpoint of boom (kg) | 158 | | | | |
| Lift capacity at endpoint of KUKA (kg) | 10 | | | | |
| Energy to charge DCP battery [kilowatt-hour (kWh)] | 12.9 | | | | |
| Energy to charge KUKA battery (kWh) | 3.6 | | | | |
| DCP runtime per battery charge (hours) | 6.5 | | | | |
| Platform width, outriggers compact (m) | 1.03 | | | | |
| Platform length, outriggers compact (m) | 5.92 | | | | |
| Platform height, outriggers compact (m) | 2.72 | | | | |
| Mean pose repeatability error for AT40GW (mm) | 13.2 | | | | |
| Mean pose repeatability SD AT40GW (mm) | 6.9 | | | | |
| Position resolution of KUKA (mm) | 0.06 | | | | |
| Maximum joint speed | AT40GW | | | | KUKA |
| | Joint 1 | Joint 2 | Joint 3 | Joint 4 | |
| | 8°/s | 6°/s | 6°/s | 120 mm/s | 225°/s |

and robotic arms. Preliminary explorations of depositing materials while driving autonomously were also conducted, as can be seen in Fig. 2A and movie S1. Further autonomy and full-body motion planning would require additional sensor feedback.

### *Energy consumption, storage, and sourcing*

The commercial AT40GW unit is built around a diesel engine and hence requires constant refueling. In the pursuit of full, self-sufficient autonomy of the platform, the DCP was outfitted with an electrical drive system, which is then rechargeable through solar panels. An electric motor connected to a second hydraulic pump was added to the system alongside two series-connected Brammo Modulithic 59/100 battery modules (fig. S3). The battery modules provide a combined 118 Vdc at 100 Ah power supply, which is sufficient to drive the DCP and all its primary functions for roughly 8 hours. Two 100-W photovoltaic panels were added to the platform, providing an alternative supplemental charging means for the main battery bank. The panels also created shade and physical protection for control electronics (fig. S4). A separate lead-acid battery system with a 5000-W inverter was powered by the solar panels to provide electricity to the KUKA robotic arm and control system. In addition to enabling power independence through remote charging, the electric motor system reduced the audible noise considerably compared with the diesel engine.

## 3D-printed insulated formwork

### *Overview*

To facilitate integration of the DCP with more traditional construction methods, a 3D-printed insulated formwork technique, termed print-in-place (*28*, *34*), was developed. The PiP process is similar to premade insulated concrete formwork (ICF) block technology, allowing the PiP process to be incorporated with traditional techniques, such as well-known finishing methods developed for formwork. By using insulated foam for the formwork, the process is a zero-waste method, because the formwork can be left in place for insulation. In contrast to direct-extrusion concrete printing, which requires using high-performance concretes with specifically optimized slump, flow characteristics, and cure time (*28*, *35*), any castable structural material can be used to backfill the produced mold (fig. S5), including locally available materials such as dirt and conventional concrete. The PiP process also enables straightforward embedding of components into the structure, because electrical wiring, plumbing, and other features can be inserted into the easily worked printed formwork before it is backfilled.

### *Material properties*

A variety of fast-curing polyurethane foams were evaluated for suitability to the PiP application. Dow Chemical's Froth-Pak insulation foam was selected on the basis of cure rate, ease of spray control, and consistency of layer deposition. The Froth-Pak Foam is a two-component polyurethane closed-cell foam commonly used in construction for thermal insulation. It begins to cure in 30 s, expands to nearly 80 times its initial volume to yield a low density of 28 kg/$m^3$, and exhibits an *R* value of 6.6 initially and 5.3 after aging. Its compressive strength is 161 kPa, tensile strength is 248 kPa, and shear strength is 88 kPa (*36*).

### *Deposition system design*

A prototype deposition system was constructed, where the two components are mixed and sprayed onto the target surface. The foam is sprayed through a replaceable mixing nozzle, allowing different flow rates and spray shapes dependent on nozzle geometry. The foam deposition head used here (fig. S6) is the second iteration of a design first completed as part of our previous work (*28*). This new iteration used 3D-printed parts from the Formlabs SLA Form 2 printer, fabricated using Formlabs Tough Resin. A servo drives the nozzle valve to control flow rate (fig. S7), and a microcontroller drives the interface box, allowing either manual or automated control via a serial port interface.

### *Additive fabrication tests*

*Basic print testing.* In preparation for architectural-scale digital fabrication using the PiP technique, several print tests were conducted. An optimal combination of foam flow rate, feed rate, and nozzle geometry was determined through extensive experimentation, as shown in fig. S8. A feed rate of 0.15 m/s with the Dow "Medium Cone" nozzle (Dow PN 259219) and a foam mixture/pressure ratio of 1.03 MPa in the polyol component/1.38 MPa in the isocyanate component was found to repeatably produce an 80-mm-wide, 35-mm-high print trace suitable for PiP applications.

These print parameters yield a volumetric fabrication rate of 1.728 $m^3$/hour. This is extremely fast in comparison with other fabrication techniques used in automated construction, which largely do not exceed 0.5 $m^3$/hour, as described below. This high print rate enables

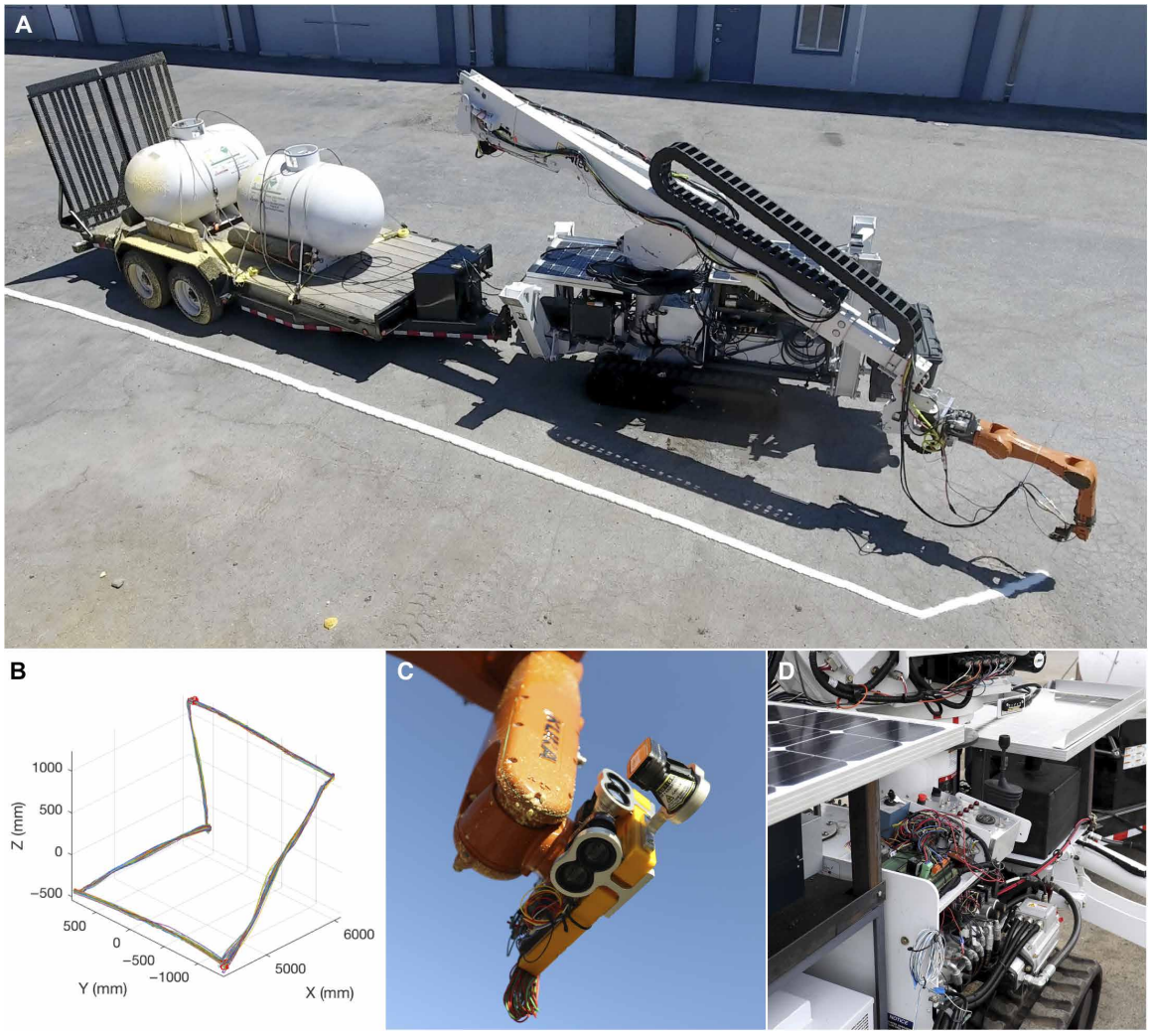


**Fig. 2. Mechanical details of the DCP.** (**A**) DCP with attached material carriage trailer, printing while driving. (**B**) Plot of measured trajectory from ISO 9283 pose repeatability characterization. (**C**) Endpoint localization sensor harness attached to end of KUKA. (**D**) Detail of photovoltaic panels, electrohydraulic pump, and hydraulic controls.

efficient automated fabrication, even at substantially larger scales than had been produced with PiP in previous work.

*Overhang print testing.* To evaluate the structural geometric complexity achievable with PiP, overhang printing tests were conducted by depositing layers of foam at a range of angles (30°, 45°, 60°, and 90°) from vertical. Successive layers were found to adhere in a consistent fashion across all angles tested, even when printing a horizontal overhang in the 90° test. A 0.5-m-tall, 1-m-long test print sample exhibiting doubly curved geometry was successfully fabricated as well (fig. S9), demonstrating the importance of overhang printing. This ability to print overhangs was later used again to directly print a horizontal bench inside a full-scale structure, described below.

*Pressure testing of printed samples.* To function as formwork, formworks printed with PiP must exhibit strong layer adhesion to maintain the hydrostatic pressure generated as concrete is poured into the formworks during casting. Foam adhesion between printed layers was tested using a custom pressure testing fixture and printed wall sections (Fig. 4C). For comparison, a traditional expanded polystyrene ICF (Reward Wall System ICF) was pressure-tested using the same test fixture. The average failure pressure of the tested printed polyurethane test sections and commercial ICFs was 53.4 and 56.8 kPa, respectively. Example data from a printed polyurethane panel test are seen in Fig. 4E. This result confirms that the printed wall structures exhibit sufficient strength to withstand the hydrostatic pressure produced during concrete casting, for pours of up to 2 m in height. Furthermore, one of the benefits of additive fabrication is the ability to customize formwork thickness. This control enables variation of wall and formwork thickness to reduce material usage and optimize insulation for where it is most effective. For particularly high pours, printed foam layers could have variable width, with wider layers near the bottom of the wall to increase strength.

*Rebar tie integration.* To facilitate integration with traditional concrete reinforcement methods, rebar ties can be inserted during the printing process. Preliminary explorations of various rebar tie designs were conducted and used in print tests as shown in Fig. 4B (*28*, *37*). A digitally controlled rebar tie inserter that deposits ties during the foam deposition process was developed and tested (fig. S10).

*Surface roughness characterization of printed samples.* Like most layer-based additive fabrication techniques, PiP fabrication produces a striated surface texture after printing. This texture contributes to the resolution of the printing process, as well as the surface finish of the

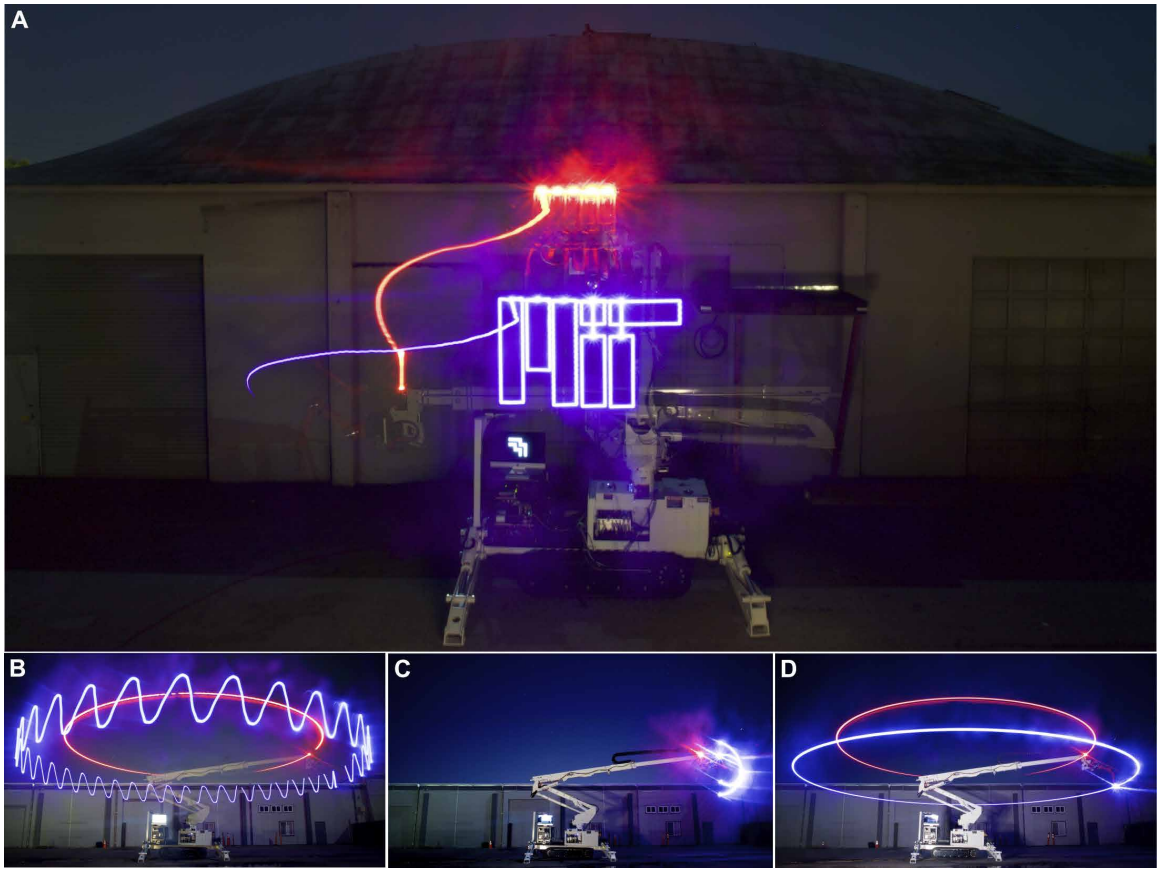


**Fig. 3. Visual record of DCP toolpaths.** (**A**) Macro arm moves between workspaces, whereas micro arm executes toolpath in each workspace to generate the MIT logo. (**B**) Micro and macro arms operate simultaneously to produce sinusoidal endpoint trajectory. (**C**) Range of motion of micro arm. (**D**) Range of motion of macro arm.

final product. To quantify the typical surface textural properties of PiP fabricated formworks, a 250 mm–by–300 mm sample of material printed in-lab using a conventional robotic arm was analyzed in accordance with ISO 4287 (*38*). A detailed description of the testing and analysis procedure is presented in text S2, and a sample waviness profile can be seen in Fig. 4D.

We find that the surface produced by the PiP process exhibits roughness with features on the order of ~1 mm. This has been observed in printing to be affected by a number of print parameters, including isocyanate/polyol mixture (a less stiff mixture spatters less), distance from spray nozzle to print surface, spray pressure, spray flow rate, and nozzle cleanliness. Meanwhile, the waviness of the PiP surface is dictated primarily by foam layer structure. In the test sample measured, layer height—which corresponds approximately to $W_{sm}$—is on the order of 40 mm. At this layer height, the total lateral deviation of the printed surface—captured in $W_t$—is on the order of 12 mm.

Further characterization is needed to explore how changes in layer height and other parameters affect this relationship. Note that these are likely best-case estimates, because the sample used was printed in ideal conditions. Larger-scale components printed with the DCP have been observed to exhibit substantial Z-waviness as well (e.g., fig. S11), generally resulting from imperfections in the starting print surface. However, this analysis provides a useful lower bound on the geometric accuracy of the PiP process, indicating what architectural components can be produced directly with PiP, and what will require additional postprocessing via subtractive machining, surface smoothing, or other methods.

### *Traditional finishing techniques*

As described above, structures fabricated with PiP are inherently rough, with a clear layered texture. However, for many applications, a rough surface finish is not problematic, because traditional construction finishing techniques for standard ICFs can be applied. Commercial ICFs exhibit rough finishes, especially around joints and layer blocks. To mitigate this, a range of typical interior and exterior finishing techniques for ICF structures are used in construction today, including various types of sprayed mixtures (stucco, plaster, shotcrete, etc.), lap siding (metal, vinyl, cement, etc.), and gypsum drywall panels. To examine use of these processes with PiP fabricated walls, a curved wall section was printed, with rebar ties inserted. The wall was then successfully finished using common finishing techniques for ICF, by applying a plaster coating to the wall, followed by belt sanding and painting (Fig. 4B).

### *Subtractive fabrication tests*

The 3D-printed foam structures are easily milled and cut, allowing automated subtractive fabrication processes to produce higher-resolution parts. As seen in the example in Fig. 4A, a printed layered panel has been linearly milled at the top. Using a combination end effector with a foam deposition head and a rotary mill enables fast switching between additive and subtractive fabrication modes (fig. S12). Figure 4F shows a concrete part cast from a mold that was 3D-printed with polyurethane foam and milled by a KUKA robotic arm, shown in fig. S13.

### *Dynamic mixing for gradient properties*

The 3D-printed foam can be used to create spatial variations in material properties, through both variations in print geometry and through

dynamic tuning of the foam's chemical mixture. With the two-component mixture used in Froth-Pak, stiffness can be varied by changing the ratio of isocyanate to polyol. Thermal insulation properties are also controllable by modulating printed wall thickness, enabling structures to be selectively insulated to produce specific thermal flows through the structure.

Additional components can be added into the mixture dynamically as the print proceeds. To explore this, an experiment was conducted, where color dye mixtures were added through a proportional valve into the spray foam polyol component before the components reached the nozzle. By modulating the flow rate of dye into the polyol, we introduced variable amounts and types of colored dye into the foam (Fig. 4G). This results in volumetric color that can be continuously graded throughout the printing process (Fig. 4H). Color variations (fig. S14) could be used for highlighting areas for construction purposes and for aesthetic value. Moreover, this experiment shows how, in the future, dynamic tuning of other material properties through proportional mixing could offer a variety of new functionalities, such as the stiffness and conductivity gradients described in (*19*).

## Case study: Architectural-scale dome

Results from preliminary tests using PiP fabrication demonstrated the potential for true architectural-scale construction using the DCP. To experimentally validate this, a full-scale structure was designed and fabricated.

The structure was designed as a hemi-ellipsoidal dome with an open top. The hemi-ellipsoidal dome used here is an interesting structural

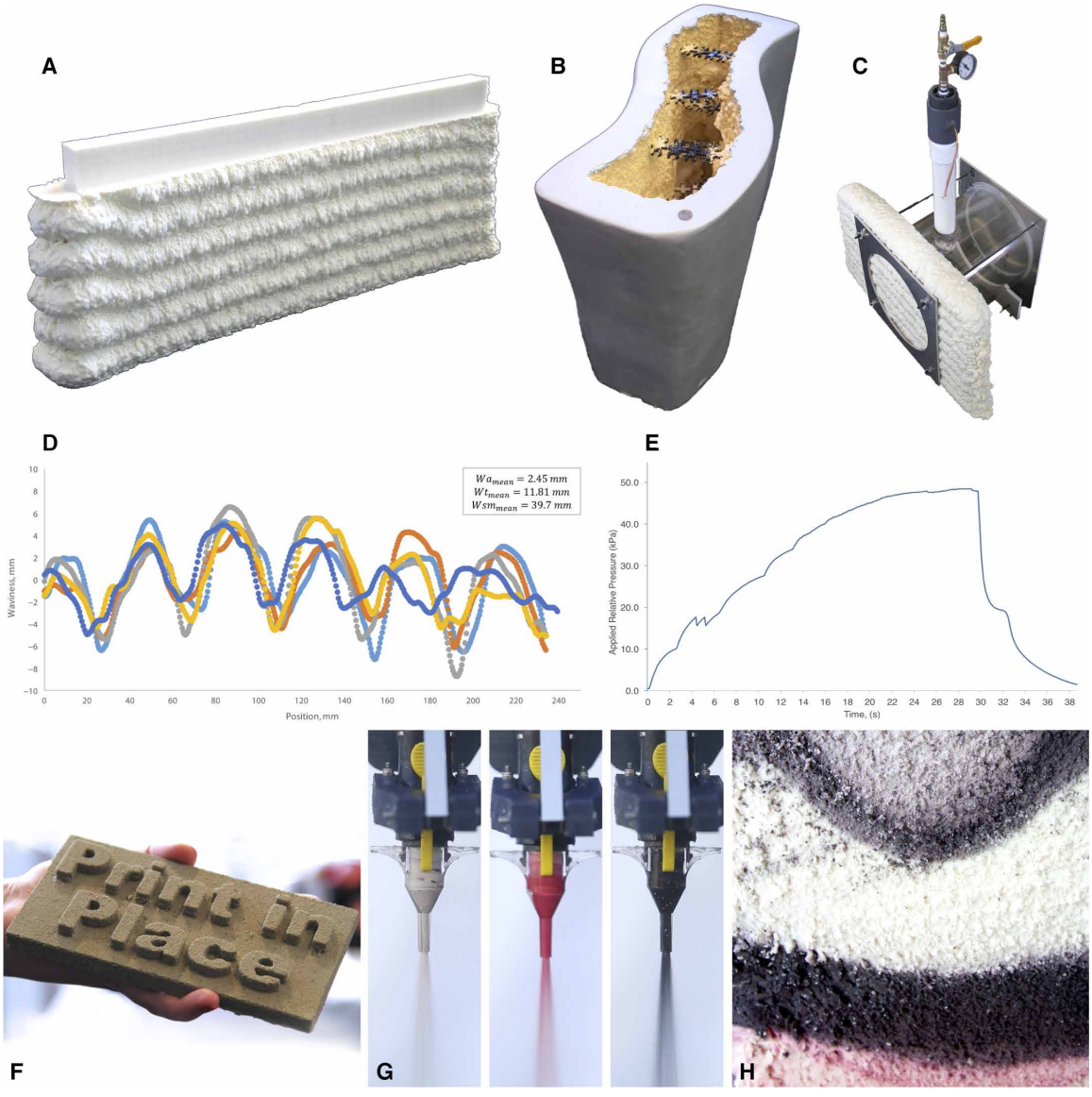


**Fig. 4. PiP fabrication.** (**A**) PiP wall section, with milled portion to improve surface finish and geometric accuracy. (**B**) Curved, 1-m-high wall section, finished with conventional ICF finishing techniques. (**C**) Hydrostatic pressure testing fixture for PiP and conventional ICF sections. (**D**) Surface waviness plots with summary statistics for PiP wall sample. (**E**) Example measured pressure curve from hydrostatic pressure testing experiments with PiP wall sections. (**F**) Artifact produced via casting into mold milled from PiP section, demonstrating feature resolution achievable in PiP foam. (**G**) Foam sprayer nozzles demonstrating dynamic mixing of foam dyes to colorize the foam. (**H**) Interior of colorized foam print, showing color gradients.

form, which, when viewed in section, has a half-circular outer contour but also a half-ellipsoidal inner contour. This causes the thickness of the wall to taper as the dome rises, reducing cast material consumption and structural weight. This structure provides a particularly compelling example of the value of automated additive construction techniques on the worksite: This section profile would be challenging to produce with conventional construction means but poses no particular difficulty for systems like the DCP.

The dome was designed to have a base diameter of 14.6 m, which was the maximum diameter structure of this design that could be accommodated in the DCP's workspace. The height of the dome section was limited to 3.7 m to ensure user access to the foam spray nozzle at all times, although the dome could have continued almost to closure before encountering kinematic limitations of the DCP. A segment of the dome wall was left open for the DCP unit to enter and exit.

***Finished structure***

This structure was successfully printed on site in Mountain View, California, during July 2016, over a period of 13.5 hours (Fig. 5 and fig. S15). The final printed formwork structure without backfill was substantial enough to support a human's weight and withstand outdoor environmental conditions (fig. S16). The dome formwork was deliberately not filled with concrete, in the interests of facilitating disposal of the structure. However, using traditional ICF techniques, the printed dome formwork could be filled with concrete or any other castable structural material to create a permanent structure.

***Printed overhang feature***

To experimentally test large-scale printed overhang features, horizontal printing was successfully demonstrated in the dome to produce a bench structure on the inside wall (fig. S17). The nozzle was rotated such that it was perpendicular to the existing vertically printed wall and moved inward horizontally with each printed layer. The rapid curing rate of the foam successfully enabled horizontal printing without any form of support material, as seen in Fig. 5B.

***Environmental conditions***

The print was completed outdoors, with no barrier/protection from ambient conditions. The temperature over the print time ranged from 13° to 27°C. Wind speed was a moderate breeze throughout the print with measurements ranging from 3.6 to 9.4 m/s. Relative humidity over the print time ranged from 42 to 78%.

Although the actual print time was under 13.5 hours, the structure took 2 days to complete because of a variety of issues that occurred during the printing process. Unexpected issues included lost encoder counts on the rotary encoder on the main base rotational joint and curing issues when a layer of morning dew settled on top of the printed foam. The high water concentration on the surface of the previously printed layer from the dew unevenly accelerated the foam curing process, causing the bond to fail and the layer to spiral off the side of the structure (fig. S11). To resolve this issue, the warped layer was pulled off, and the morning sun quickly dried the dew off, allowing a properly printed layer to be deposited shortly after.

## DISCUSSION

The results of these experimental characterization and fabrication tests demonstrate that the DCP platform carries exciting potential to revolutionize construction. Our mobile robotic platform has demonstrated on-site, continuous 3D printing of an architectural-scale structure. Furthermore, the structure was fabricated using a technique of printing insulating formwork that offers extremely rapid fabrication rates; enables the use of common structural materials rather than relying on process-specific formulations; can be finished using well-understood, existing techniques; and has the potential to substantially reduce barriers to adoption because of its similarity to existing ICF construction techniques. The executed design uses complex curvature and variable wall thickness to achieve an efficient structure that would be extremely difficult to produce with traditional construction techniques. We believe that, at the time of writing, this printed test structure is currently both the largest monolithic structure ever 3D-printed by an on-site mobile platform and the fastest autonomously printed architectural-scale structure.

### Comparisons with existing construction methods

Leveraging digital manufacturing techniques to create buildings would enable novel structural designs, improved structural performance, and greater construction efficiency. Use of 3D printing techniques would change the cost structure of buildings to be based on total raw material cost, rather than on geometric complexity. With these techniques, architects can create low-cost structures that are more functional, unique, and more versatile than those possible through traditional techniques. Automation of the construction process also simplifies logistics, reduces construction time, and decreases labor costs. Having a correct time prediction is also very useful for planning purposes and ensuring that a project finishes on time. Automation of the building process also eliminates the scheduling difficulties of having multiple contractors on a job site at the same time and saves construction time and, consequently, labor costs. Last, robotic construction would decrease the number of injuries and deaths in the construction industry by reducing human exposure to many of the dangerous and laborious tasks involved in constructing a building.

As an example, a preliminary financial analysis was conducted to compare printed insulated formwork with traditional construction methods for an average-sized one-story rectilinear house. Estimates from construction workers were used to calculate costs for wooden construction and ICF construction, and included human labor for operating the PiP deposition system. For the purpose of the estimate, finishing costs and interior walls were not considered for all techniques, and the added long-term financial benefit of the thermal insulation for energy savings was not considered. This analysis shows that the cost of printing the formwork of a house with the PiP method would be 8% less expensive than traditional wood construction methods and 31% less expensive than regular ICF construction (*28*). Most of these cost savings come from labor costs, but transportation volume costs (defined as the volume required to transport construction materials to the worksite) are also substantially smaller for PiP structures than for ICF construction because of PiP foam's high expansion rate from liquid to solid. Additional details on the financial analysis can be found in the Supplementary Materials (text S3) (*37*). These estimates strongly support the fiscal feasibility for the printed formwork technique, showing that it will not only save time and increase safety but also lower costs for even simple rectilinear buildings. For buildings with complex geometry, such as walls with curvature, overhangs, and optimized variable wall thickness, the cost for the PiP process would remain the same as the cost for a rectilinear building, whereas the cost to produce the complex geometry with traditional construction processes would be exponentially higher.

### Comparisons with existing automated construction research

An important lens for evaluating the contributions of the DCP is in the context of other large-scale automated construction systems that exist

today. However, the diversity of automated construction systems in development today makes it challenging to find a common set of metrics for intersystem comparison. In addition to variations in system size and intended task, automated construction systems have been designed to leverage a huge range of fabrication processes, which are frequently difficult to compare.

In light of these challenges, we propose a basic analysis using two metrics that can provide some insight into the relative performance of different automated construction systems and that can be easily estimated if exact values have not been published for a given system. The first metric is the total work volume that the system can reasonably reach during a fabrication operation. This estimates the scale of the structures that a given system can produce. The second metric is the typical maximum volumetric fabrication rate a system can achieve with its default fabrication process.This provides a measure of how rapidly a given system can produce structures. Together, these two metrics give a rough sense of a system's overall performance in executing automated construction tasks.

Table 2 lists these metrics for a selection of automated construction systems that either are in active development or have been developed within the past 5 years (*39*). Systems are also classified (i) by type, as either gantry-, arm-, or swarm-based systems; (ii) as mobile or static; (iii) by whether they are intended for on- or off-site fabrication; and (iv) by fabrication modality, with primary fabrication media listed.

Last, we list the enclosed volume of the largest structure fabricated with a given system/process combination that we have been able to identify in the literature. In cases where metrics are not explicitly published, we have had to estimate from other available data: Further details of how estimations were generated for each system are available in text S4. The metrics listed here are of course not immutable: A gantry's work volume could be expanded, or a high-throughput fabrication technique could be implemented on a new system. Although Table 2 is useful for comparing current automated construction systems as they have been reported in the literature, it does not reflect intrinsic performance limits.

As this table demonstrates, the DCP occupies an interesting position in this landscape of automated construction systems. First, the work volume of arm-based systems like the DCP generally exceeds that of static gantry-based systems and even the practical workspace of swarm-based systems. Particularly, as arm-based systems become increasingly mobile—as the In-Situ Fabricator project has demonstrated (*15*)—the work volumes of arm-based systems will continue to grow. Second, this mapping shows that the DCP's primary fabrication system—PiP construction—substantially outperforms other fabrication techniques in terms of volumetric fabrication rate, largely because of the extremely high expansion rate of the polyurethane foam. Although this metric does not include any time required for secondary operations, such as pouring concrete or finishing exterior surfaces,

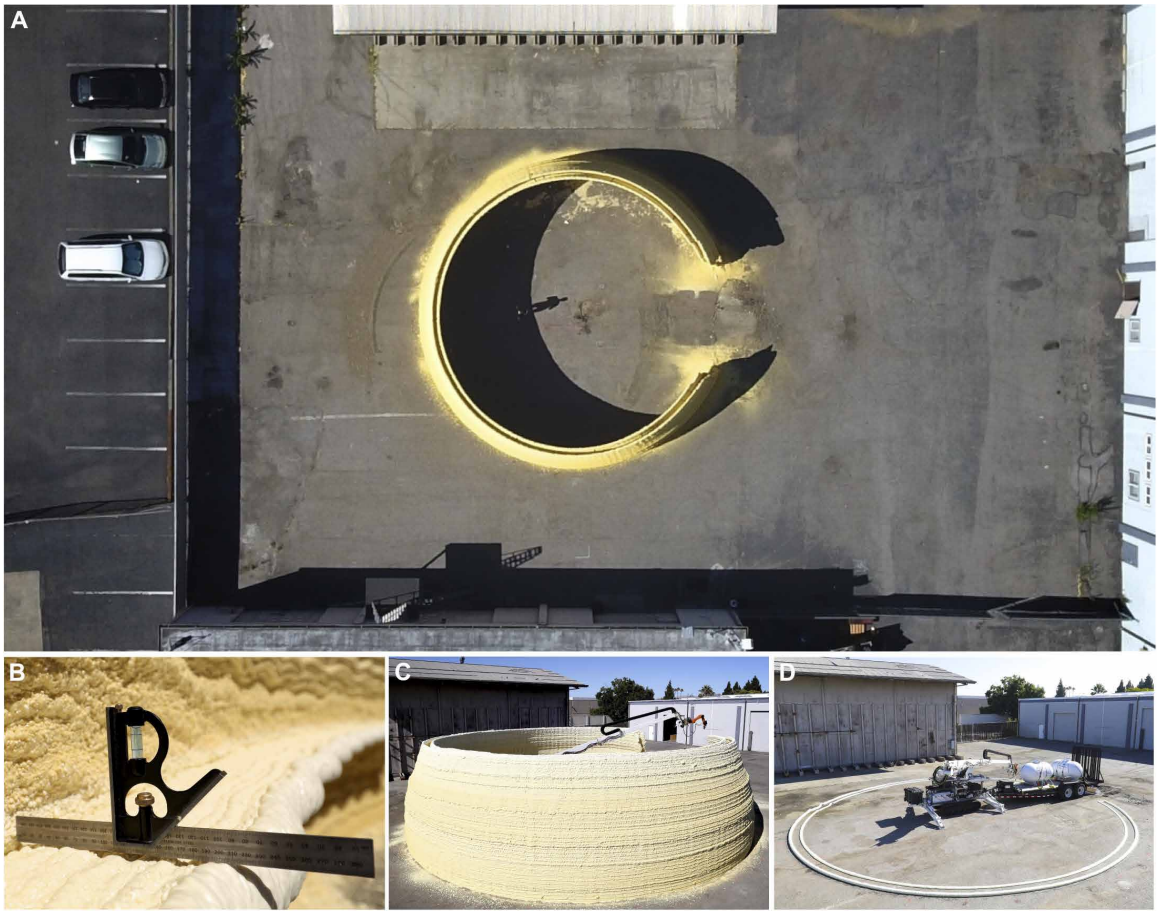


**Fig. 5. Architectural-scale hemi-ellipsoidal dome section case study.** (**A**) Open dome, top view. (**B**) View of horizontal bench structure, fabricated as an overhang feature without support material on the inside of dome wall. (**C**) Completed structure, side view. (**D**) Beginning of 3D print, showing DCP with trailer.

**Table 2. Comparison of existing automated construction research.** In many cases, data for metrics reported here were not directly available, and estimates have been made using other references. Please see text S4 for further explanation of methodology, particularly for entries marked with asterisks.

| Automated construction system name | Developer | Primary fabrication media | Quantitative metrics | | | Qualitative metrics | | | |
|---|---|---|---|---|---|---|---|---|---|
| | | | Largest fabricated structure ($m^3$) | Total work volume ($m^3$) | Typical volumetric fabrication rate ($m^3$/hour) | System classification | Fabrication modality | System mobility | Fabrication |
| DCP | Mediated Matter—MIT | Spray-foam insulation formwork | 565 | 2786 | 1.728 | Arm | Extrusion | Mobile | On-site |
| Apis Cor | Apis Cor | Concrete extrusion | 396 | 434 | 0.375 | Arm | Extrusion | Static | On-site |
| In-Situ Fabricator | ETH Zurich | Brick assembly | 9.75 | 34.7 | 0.176 | Arm | Assembly | Mobile | On-site |
| Hadrian 105 | Fastbrick Robotics | Brick assembly | 9.22 | 45976 | 0.433 | Arm | Assembly | Mobile | On-site |
| Guedel Gantry Robot | ERNE AG/ETH Zurich | Timber assembly | 52.2 | 556 | 0.718 | Gantry | Assembly | Static | Off-site |
| BAAM | Cincinnati Incorporated/Oak Ridge National Laboratory | Thermoplastic | 4.42 | 32.3 | 0.033 | Gantry | Extrusion | Static | Off-site |
| 3DCP | Eindhoven University of Technology | Concrete extrusion | 1.25 | 113 | 0.144 | Gantry | Extrusion | Static | Off-site |
| Concrete Printing | Loughborough University | Concrete extrusion | 0.86 | 128 | 0.090 | Gantry | Extrusion | Static | Off-site |
| Contour Crafting | University of Southern California | Concrete extrusion | 0.14 | 55.7* | 0.018 | Gantry | Extrusion | Static | Off-site |
| Flight Assembled Architecture | ETH Zurich | Foam block assembly | 57.7 | 1000 | 0.375 | Swarm (aerial) | Assembly | Mobile | On-site |
| Minibuilders | Institute for Advanced Architecture of Catalonia | Polymer-bonded marble powder | 1.50 | 1.50* | 0.015 | Swarm (terrestrial) | Extrusion | Mobile | On-site |

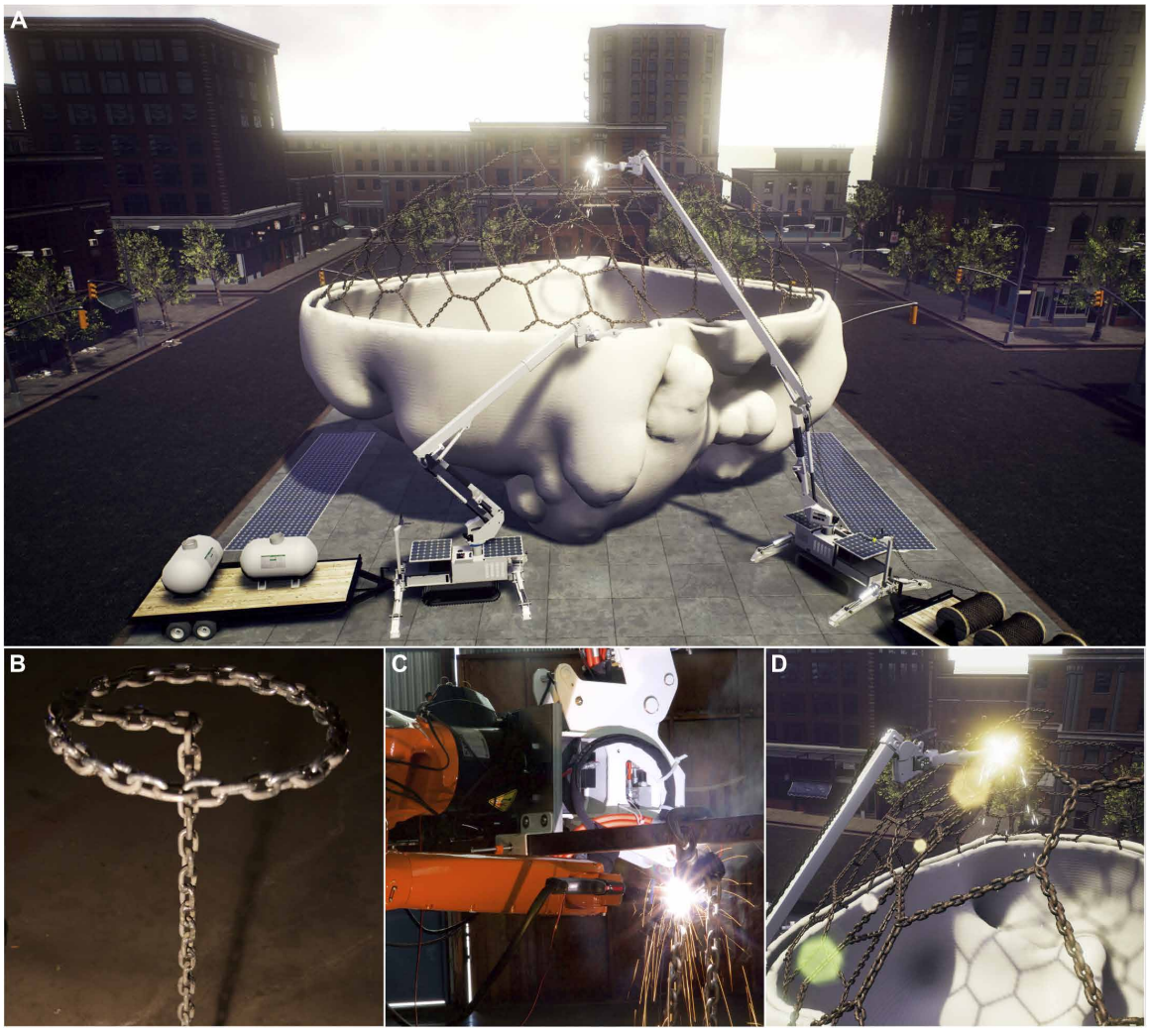


**Fig. 6. Future worksite integrations for the DCP.** (**A**) Rendering of DCP systems fabricating architectural-scale structure in urban environment, using combined PiP and robotic chain welding fabrication. (**B**) Manually fabricated welded chain stool structure. (**C**) Automated fabrication of welded chain structures using the DCP. (**D**) Rendering detail, showing DCP performing welded chain fabrication.

the speed advantage that PiP fabrication holds suggests that even with secondary operations taken into consideration, the process will still perform substantially better than competing alternatives. This validates the PiP concept and strongly suggests that fabrication techniques that can leverage high-volume elements like spray polyurethane foam are well adapted to automated construction tasks.

The limitations of this analysis are also instructive to examine. Particularly, this analysis reduces the performance of a given system and fabrication process to two primary metrics, which may obscure other important characteristics, such as mechanical performance of the finished structure or the resolution of a given fabrication process. There is clearly a need for a standardized test artifact—similar in intent to the product-scale additive manufacturing test artifact proposed by Moylan *et al.* (*40*) but optimized for architectural applications—that can be used to characterize and compare the performance of different automated construction systems across a wide range of metrics. Developing this type of artifact is an exciting challenge for the automated construction community and one that we look forward to contributing to in our future work.

## Future directions

Moving forward from our successful proof-of-concept demonstration of the DCP and the PiP fabrication technique's potential, our future research directions include further integration of the developed system into existing construction sites and exploration of expanding the DCP's ability to operate self-sufficiently.

### *Integration into existing construction sites*

The PiP fabrication process is well suited for deployment within existing construction sites, because it can be used in place of traditional insulated formwork. We have demonstrated the PiP process to several ICF contractors, who confirmed that a variety of traditional finishing techniques for ICFs could be used on formwork constructed with the PiP process. The contractors we spoke with were also excited by its capabilities to customize geometries, vary insulation widths, and limit casting leaks that often occur in current ICF construction.

The integration of the DCP and PiP process into existing construction workflows is a key step forward, because the construction industry has enormous inertia and implements new technologies very conservatively. We look forward to engaging the DCP with real-world projects, which

will facilitate long-term tests of the robustness, environmental impact, and safety of structures produced with the PiP method. In parallel, we plan to continue development of additional sensor systems and control techniques to improve resolution, accuracy, and dynamic performance of the DCP system.

In the future, we plan to develop additional techniques using traditional construction materials to integrate with the PiP process. As an example, we have started early experimental explorations of robotic chain welding and direct arc welding of metal, which could be used in place of rebar for the PiP process and other structural applications (Fig. 6, B and C, and fig. S18).

***Toward self-sufficiency***

In the long term, the DCP is designed for the future goal of self-sufficient operation through mobility, energy sourcing through photovoltaics, and the ability to gather and use local materials in manners adaptive to the environment through on-site sensing (fig. S19). To explore these future possibilities, a series of early explorations using the DCP were constructed, demonstrating local material gathering through excavation (fig. S20), solar charging with deployable rollable photovoltaics (fig. S21), collection of on-site environmental data (radiation measurements) (fig. S22), and construction with local materials. Preliminary fabrication explorations resulted in direct arc sintering of sand (simulated with soda ash glass particles), thermally deposited ice structures, and compressed earth forms (fig. S23).

Overall, the early explorations highlight the vast future directions for digital construction. Potential benefits include novel functionality, customization, speed, safety, cost, dynamic structures, and much more. We believe that this is just the beginning of a new intermixed age of robotics, fabrication, and self-sufficiency.

## MATERIALS AND METHODS

The primary objective of this study was to explore optimal techniques for robotic fabrication at architectural scales. This was implemented through the development of a prototype robotic arm system, the DCP; explorations of a range of fabrication processes that could be implemented with this system; and, last, the execution of a case study in which a 14.6-m-diameter open dome section was fabricated with the DCP.

### DCP platform components and architecture

The DCP was controlled through a computer using feedback from mounted sensors on the system joints. Balluff BTL6 Micropulse linear position sensors were mounted to the hydraulic cylinder joints (fig. S24), and a YUMO E6B2 rotary encoder was attached to the hydraulic motor driving the rotary joint at the base of the unit (fig. S25). Beckhoff input/output modules were connected via EtherCAT to the KUKA controller for real-time input from laser distance sensors (SICK DT35 and LightWare SF30), accelerometers (Analog Devices ADXL335), gyrometers (STMicroelectronics LSM9DS1), magnetometers (STMicroelectronics LSM9DS1), and environmental sensors such as a Geiger counter (SparkFun SEN-11345). A board with these sensors was attached to the end of the KUKA arm (fig. S26) in addition to a variety of end effectors. The diagram in fig. S27 provides an overview of the major sensor components.

For generating tool paths for digital fabrication using the DCP, a Python program called HomePrint was designed and coded in our previous work (*28*). The program allows the input of CAD files (.STL format) plus process variables such as layer thickness, speed, and other parameters, and outputs either Cartesian tool path code or KUKA Robot Language (KRL) code through a graphic user interface (fig. S28). HomePrint included model slicing code (wxBlackcat) by Liu (*41*).

The AT40GW was controlled via pulse-width modulation (PWM) signals output by a LabJack T7 Pro DAQ unit, which communicated with the proportional hydraulic valve drivers on the AT40GW. Control of the arm was performed on a per-joint basis, using a simple feedforward velocity/PID position controller. A diagram of the control architecture used is seen in fig. S29. The feedforward control loop used velocity maps that we generated to determine which PWM values to send for specific velocities dependent on current position, due to differences based on height and extension positions of the system. In addition, velocity maps for movements with different power sources were produced to record the velocities when powered by the diesel engine hydraulic pump or the electric motor hydraulic pump.

Joint-space toolpaths were generated through a custom MATLAB toolchain. This toolchain used Corke's Robotics, Vision and Control toolbox (*42*). Task-space coordinates were produced through HomePrint or created through MATLAB scripts for more basic geometries.

The KUKA electric arm was controlled in three different modes: KRL programs triggered by MATLAB through the LabJack and the Beckhoff input/output models, external control from MATLAB of joint angles or Cartesian coordinates through the Robot Sensor Interface (RSI), and internal control from sensors attached to the Beckhoff I/O modules via the RSI system.

For external laser characterization of the aerial lift in accordance with ISO 9283:1998, a mount for the Leica retroreflector was constructed and attached to the end of the KUKA for testing (fig. S30). Laser measurements were recorded at a frequency of 3.3 Hz. The worst-case measurement accuracy of the AT901 was 0.0141 mm. Analysis of ISO 9283:1998 pose repeatability data was completed using a custom MATLAB script in accordance with the ISO standard; further details of this analysis are available in text S1.

### DCP end effectors

End effectors developed for the DCP included a foam deposition head, a metal chain welding system, a bucket excavator, a hedge trimmer, and a chainsaw. A variety of end effector tools used with the system are seen in figs. S31 and S32. End effectors that incorporate some electromechanical mechanism, such as the metal chain welding system, were connected to a relay board triggered by the LabJack, allowing digital control.

## SUPPLEMENTARY MATERIALS

robotics.sciencemag.org/cgi/content/full/2/5/eaam8986/DC1

Text S1. ISO 9283-1998 pose repeatability characterization.
Text S2. ISO 4287 surface roughness characterization.
Text S3. Preliminary financial analysis of PiP construction.
Text S4. Notes on estimations in construction robots comparison table.
Table S1. ISO 4287 surface topography summary data.
Fig. S1. Laser compensation enabling maintenance of constant aboveground height.
Fig. S2. KUKA endpoint position during programmed oscillatory movement with laser sensor compensation vs. without laser compensation.
Fig. S3. Electrohydraulic drivetrain.
Fig. S4. Solid PV panels.
Fig. S5. PiP mold filled with conventional concrete.
Fig. S6. Foam deposition head for PiP fabrication.
Fig. S7. Foam deposition head detail.
Fig. S8. Empirical determination of optimal foam extrusion parameters.
Fig. S9. Doubly curved geometries fabricated with PiP process.
Fig. S10. Automated rebar tie inserter prototype.
Fig. S11. Adhesion failure caused by excessive moisture on the printed surface from the dew condensation that occurred in the morning during printing.
Fig. S12. KUKA robot arm with combined milling/PiP fabrication end effector.

Fig. S13. Milled spray polyurethane foam mold used to produce concrete casting shown in Fig. 4F.
Fig. S14. Range of color variation in spray polyurethane foam insulation.
Fig. S15. Completed PiP dome.
Fig. S16. The PiP dome was able to support human weight, even without any structural material (such as concrete) cast inside the formwork.
Fig. S17. Fabrication of horizontally printed overhang feature.
Fig. S18. Fabrication using direct welding deposition technique.
Fig. S19. Concept computer renderings of future applications for DCP systems.
Fig. S20. Excavation tests with the DCP demonstrating both subtractive site preparation and local material gathering.
Fig. S21. A rollable photovoltaic panel was used for testing with the DCP to explore deployable large solar arrays for power self-sufficiency.
Fig. S22. Radiation scanning using a Geiger counter mounted to the DCP to gather volumetric data around three radioactive sources.
Fig. S23. Preliminary fabrication explorations with electrosintered powdered glass, thermally deposited ice structures, and compressed earth forms.
Fig. S24. Balluff magnetostrictive sensors.
Fig. S25. YUMO rotary encoder.
Fig. S26. Sensor board that mounts at the end of the KUKA robotic arm.
Fig. S27. DCP sensor architecture diagram.
Fig. S28. HomePrint software interface.
Fig. S29. DCP control architecture diagram.
Fig. S30. Leica retroreflector mounted to the KUKA robotic arm on the DCP.
Fig. S31. A selection of various DCP end effectors.
Fig. S32. Thermoplastic fabrication end-effector and 3D printed structure made from acrylonitrile butadiene styrene (ABS).
Movie S1. Short video overview of the DCP.
References (*43*–*66*)

## REFERENCES AND NOTES


1. Construction Intelligence Center, *Global Construction Outlook 2020* (Construction Intelligence Center, 2015).
2. International Labour Organization, *Facts on Safety at Work* (International Labour Organization, 2005).
3. T. A. Edison, Apparatus for the production of concrete structures, U.S. Patent 1326854 (1919).
4. International Association for Automation and Robotics in Construction, *Robots and Automated Machines in Construction* (International Association for Automation and Robotics in Construction, 1998).
5. I. Smith, S. Wamuziri, M. Taylor, Automated construction in Japan. *Proc. Inst. Civil Eng. Civil Eng.* **156**, 34–41 (2003).
6. E. Gambao, C. Balaguer, A. Barrientos, R. Saltaren, E. A. Puente, Robot assembly system for the construction process automation, *Proceedings of International Conference on Robotics and Automation (ICRA 1997)*, Albuquerque, NM, 25 April 1997, pp. 46–51.
7. G. Pritschow, M. Dalacker, J. Kurz, M. Gaenssle, Technological aspects in the development of a mobile bricklaying robot. *Autom. Constr.* **5**, 3–13 (1996).
8. V. Helm, S. Ercan, F. Gramazio, M. Kohler, Mobile robotic fabrication on construction sites: DimRob, *IEEE International Conference on Intelligent Robots and Systems (IROS 2012)*, Algarve, Portugal, 7 to 12 October 2012, pp. 4335–4341.
9. B. Shirinzadeh, G. Alici, C. W. Foong, G. Cassidy, Fabrication process of open surfaces by robotic fibre placement. *Robot. Comput. Integr. Manuf.* **20**, 17–28 (2004).
10. S. Lim, R. A. Buswell, T. T. Le, S. A. Austin, A. G. F. Gibb, T. Thorpe, Developments in construction-scale additive manufacturing processes. *Autom. Constr.* **21**, 262–268 (2012).
11. B. Khoshnevis, Automated construction by contour crafting—Related robotics and information technologies. *Autom. Constr.* **13**, 5–19 (2004).
12. F. P. Bos, R. J. M. Wolfs, Z. Y. Ahmed, T. A. M. Salet, Additive manufacturing of concrete in construction: Potentials and challenges of 3D concrete printing. *Virtual Phys. Prototyp.* **11**, 209–225 (2016).
13. F. Augugliaro, S. Lupashin, M. Hamer, C. Male, M. Hehn, M. Mueller, J. Willmann, F. Gramazio, M. Kohler, R. D'Andrea, The flight assembled architecture installation: Cooperative construction with flying machines. *IEEE Control Syst.* **34**, 46–64 (2014).
14. F. Augugliaro, A. Mirjan, F. Gramazio, M. Kohler, R. D'Andrea, Building tensile structures with flying machines, *IEEE International Conference on Intelligent Robots and Systems (IROS 2013)*, Tokyo, Japan, 3 to 7 November 2013, pp. 3487–3492.
15. T. Sandy, M. Giftthaler, K. Dörfler, M. Kohler, J. Buchli, Autonomous repositioning and localization of an in situ fabricator, *IEEE International Conference on Robotics and Automation (ICRA 2016)*, Stockholm, Sweden, 16 to 21 May 2016, pp. 2852–2858.
16. N. Labonnote, A. Ronnquist, B. Manum, P. Rüther, Additive construction: State-of-the-art, challenges and opportunities. *Autom. Constr.* **72**, 347–366 (2016).
17. N. Legmpelos, thesis, Massachusetts Institute of Technology (2013).
18. T. C. Nguyen, "Yes, that 3D-printed mansion is safe to live in," *Washington Post*, 5 February 2015; www.washingtonpost.com/news/innovations/wp/2015/02/05/yes-that-3d-printed-mansion-is-safe-to-live-in/?utm_term=.3fcfa03e4e2c.
19. H. Strauss, The potential of additive manufacturing for facade constructions, thesis, Delft University of Technology (2013).
20. Robohub, *Hadrian Bricklaying Robot* (Robohub, 2016); http://robohub.org/robots-hadrian-bricklaying-robot/.
21. Apis Cor, Technical specifications of construction 3D printer; http://apis-cor.com/en/faq/texnicheskie-xarakteristiki-3d-printera/.
22. Gramazio Kohler Research, *Robotic Fabrication Laboratory* (Gramazio Kohler Research, 2016); http://gramaziokohler.arch.ethz.ch/web/e/forschung/186.html.
23. S. Jokic, P. Novikov, S. Maggs, D. Sadan, S. Jin, C. Nan, Robotic positioning device for three-dimensional printing. arXiv Prepr. arXiv 1406.3400 (2014).
24. M. Giftthaler, T. Sandy, K. Dörfler, I. Brooks, M. Buckingham, G. Rey, M. Kohler, F. Gramazio, J. Buchli, Mobile robotic fabrication at 1:1 scale: The in situ fabricator. arXiv:1701.03573 (2017).
25. Q J. Lindsey, D. Mellinger, V. Kumar, Construction of cubic structures with quadrotor teams, *Proceedings of Robotics, Science and Systems VII*, Los Angeles, CA, 27 to 30 June 2011.
26. In this analysis, we typically group gantry and cable-actuated systems together. Our rationale is that they share many characteristics, including fixed work volumes and limited kinematic flexibility, even if their specific kinematics differ.
27. S. Keating, N. A. Spielberg, J. Klein, N. Oxman, A compound arm approach to digital construction: A mobile large-scale platform for on-site sensing, design, and digital fabrication, in *Robotic Fabrication in Architecture, Art and Design 2014,* W. McGee, M. Ponce de Leon, Eds. (Springer, 2014), pp. 99–110.
28. S. J. Keating, M.Sc. thesis, Massachusetts Institute of Technology (2012).
29. A. Sharon, N. Hogan, D. E. Hardt, The macro/micro manipulator: An improved architecture for robot control. *Robot. Comput. Integr. Manuf.* **10**, 209–222 (1993).
30. A. M. Lytle, K. S. Saidi, NIST research in autonomous construction. *Auton. Robots* **22**, 211–221 (2007).
31. J. Y. Lew, D. J. Trudnowski, M. S. Evans, D. W. Bennett, Micro manipulator motion control to counteract macro manipulator structural vibrations, *American Nuclear Society 6th Topical Meeting on Robotics and Remote Systems Meeting*, Monterey, CA, 5 to 10 February 1995.
32. K. Yoshida, B. Wilcox, Space robots and systems, in *Springer Handbook of Robotics* (Springer, 2008), pp. 1031–1063.
33. International Standards Organization, *ISO 9283-1998* (International Organization for Standardization, 1998).
34. S. Keating, N. Oxman, Compound fabrication: A multi-functional robotic platform for digital design and fabrication. *Robot. Comput. Integr. Manuf.* **29**, 439–448 (2013).
35. T. T. Le S. A. Austin, S. Lim, R. A. Buswell, A. G. F. Gibb, T. Thorpe, Mix design and fresh properties for high-performance printing concrete. *Mater. Struct.* **45**, 1221–1232 (2012).
36. Dow Chemical, *FROTH-PAK™ Foam Insulation Product Information Sheet* (Dow Chemical, 2017); http://msdssearch.dow.com/PublishedLiteratureDOWCOM/dh_0973/0901b803809731e8.pdf?filepath=styrofoam/pdfs/noreg/179-04478.pdf&fromPage=GetDoc.
37. S. J. Keating, Ph.D. thesis, Massachusetts Institute of Technology (2016).
38. International Standards Organization, *ISO 4287-1997* (International Organization for Standardization, 1997).
39. The WinSun Company's concrete printing system has been excluded from this analysis. Although the WinSun system is certainly an important feature of the automated construction landscape today, the lack of verifiable information available about the WinSun system's performance is notable and has led other authors (*16*, *18*) to treat their work with skepticism. We consequently have elected to exclude the WinSun system from our analysis.
40. S. Moylan, J. Slotwinski, A. Cooke, K. Jurrens, M. A. Donmez, Proposal for a standardized test artifact for additive manufacturing machines and processes, in *Solid Freeform Fabrication Symposium Proceedings*, Austin, TX, 6 to 8 August 2012, pp. 902–920.
41. Z. Liu, wxBlackcat (computer program) (2009); https://code.google.com/archive/p/wxblackcat/.
42. P. Corke, Robotics Toolbox 9.10 for MATLAB (2015).
43. K. Dörfler, T. Sandy, M. Giftthaler, F. Gramazio, M. Kohler, J. Buchli, Mobile robotic brickwork—Automation of a discrete robotic fabrication process using an autonomous mobile robot, in *Robotic Fabrication in Architecture, Art and Design* (Springer, 2016), pp. 205–217.
44. Apis Cor, *The First On-Site House Has Been Printed in Russia* (Apis Cor, 2017); http://apis-cor.com/en/about/news/first-house.
45. Fastbrick Robotics, *Fastbrick Robotics: Hadrian 105 Time Lapse* (Fastbrick Robotics, 2016); www.youtube.com/watch?v=4YcrO8ONcfY.
46. M. Pivac, *Fastbrick Robotics | North American Presentations August 2016* (FastBrick Robotics, 2016); www.asx.com.au/asxpdf/20160810/pdf/4396m6dzsgd66t.pdf.

47. S. Lim, R. A. Buswell, P. J. Valentine, D. Piker, S. A. Austin, X. De Kestelier, Modelling curved-layered printing paths for fabricating large-scale construction components. *Addit. Manuf.* **12**, 216–230 (2016).
48. D. Hwang, B. Khoshnevis, Concrete wall fabrication by contour crafting, *ISARC 2004 21st International Symposium on Automation and Robotics in Construction*, Jeju Island, Republic of Korea, 21 to 25 September 2004.
49. C. Hewitt, *Why Design Now?: Contour Crafting* (YouTube, 2010); www.youtube.com/watch?v=-yv-IWdSdns.
50. TEDx Talks, *TEDxMedellin - Behrokh Khoshnevis - Robotic Construction by Contour Crafting* (YouTube, 2012); www.youtube.com/watch?v=SLIwaIOKfYc.
51. WinSun, www.yhbm.com/.
52. TU Eindhoven, Photo gallery—TU Eindhoven 3D Concrete Printing; www.tue.nl/en/university/departments/built-environment/research/research-programs/structural-design/research/research-areas/concrete-research-areas/3d-concrete-printing/photo-gallery/.
53. 3ders.org, TU Eindhoven students unveil stylish 2m tall 3D printed concrete pavilion, 3D Printer News and 3D Printing News (2016); www.3ders.org/articles/20160627-tu-eindhoven-students-unveil-stylish-2m-tall-3d-printed-concrete-pavilion.html.
54. SOM, *AMIE 1.0* (SOM, 2016); www.som.com/projects/amie.
55. Oak Ridge National Laboratory, *AMIE Demonstration Project* (Oak Ridge National Laboratory, 2016); http://web.ornl.gov/sci/eere/amie/.
56. Cincinnati, *2016 BAAM Fact Sheet* (Cincinnati, 2016); http://wwwassets.e-ci.com/PDF/Products/baam-fact-sheet.pdf.
57. L. J. Love, C. E. Duty, *Cincinnati Big Area Additive Manufacturing (BAAM)* (CRADA report ORNL/TM-2015/100, Oak Ridge National Laboratory, 2015).
58. S. Jokic, P. Novikov, *Minibuilders—How to 3d Print Big Structures with Small Robots* (2015); www.instructables.com/id/Minibuilders-How-to-3d-print-big-structures-with-s/?ALLSTEPS.
59. S. Jokic, J. Leland, Email Correspondence 2017-03-21 (2017).
60. ETH Zurich, Flying Machine Arena; http://flyingmachinearena.org/.
61. M. Krammer, Individual serialism through the use of robotics in the production of large-scale building components, in *Robotic Fabrication in Architecture, Art and Design 2016* (Springer, 2016), pp. 460–467.
62. A. A. Apolinarska, R. Bärtschi, R. Furrer, F. Gramazio, M. Kohler, Mastering the "sequential roof": Computational methods for integrating design, structural analysis, and robotic fabrication, in *Advances in Architectural Geometry 2016* (Hochschulverlag an der ETH Zürich, 2016), pp. 240–258.
63. J. Willmann, M. Knauss, T. Bonwetsch, A. A. Apolinarska, F. Gramazio, M. Kohler, Robotic timber construction—Expanding additive fabrication to new dimensions. *Autom. Constr.* **61**, 16–23 (2016).
64. ERNE AG Holzbau, *ERNE Portalroboter - Gantry Robot* (YouTube, 2015); www.youtube.com/watch?v=yOYMtLmCYuI.
65. A. A. Apolinarska, M. Knauss, F. Gramazio, M. Kohler, The sequential roof, in *Advancing Wood Architecture: A Computational Approach*, A. Menges, T. Schwinn, O. D. Krieg, Eds. (Routledge, 2016).
66. Digital Surf, *MountainsMap* (Digital Surf, 2017); www.digitalsurf.fr/en/index.html.


**Acknowledgments:** We thank Google Inc., who provided facilities in addition to supporting this project financially. We would also like to thank the following companies for their donations of material and expertise that helped make this project possible: Altec Inc., for providing the AT40GW aerial lift vehicle used in the DCP system described in this paper, as well as the L42M aerial lift vehicle that was used in the first iteration of the DCP system; Dow Chemical, for donating the Froth-Pak foam insulation used in the construction of the full-scale structure described here; BASF, for donations of material used during the development of the PiP process; Terraloom, for their assistance in generating rendered images of the DCP platform; and Autodesk Inc., for providing facilities and support to the DCP project. We thank D. Wallace, W. Flowers, and D. Trumper for advisement and the many undergraduate researchers who have helped support this work over the years, including N. Spielberg, J. Haip, G. Sellers, H. Barrett, J. Goodman, L. DeScioli, S. Gano, and D. Martin. Last, we thank the staff of the Massachusetts Institute of Technology (MIT), the MIT Media Lab, the MIT Mechanical Engineering Department, and the MIT Center for Bits and Atoms for their helpful support and for the use of their facilities. **Funding:** Support for this project was provided by Google Inc. (MIT grant no. 6933535) and through Media Lab Consortium funding (MIT grant no. 6927725).
**Author contributions:** S.J.K. led the design, construction, and testing of the first and second prototypes of the DCP and the various material deposition techniques. J.C.L. developed the low-level control architecture, interface, and portions of the software architecture (including forward and inverse kinematics) for the DCP system and supported system development, testing, and the architectural-scale print. L.C. developed the high-level software architecture, portions of the control system, and trajectory planning algorithms and supported testing and the architectural-scale print. N.O. is the director of the research group and guided the project from concept to fully functional prototype through her vision, guidance, and performance-based design principles. **Competing interests:** S.J.K. and N.O. are inventors on patent application US20130295338A1, "Methods and apparatus for computer-assisted spray foam fabrication." The other authors declare that they have no competing interests.
**Data and materials availability:** The software toolchain used to control the DCP is available under the MIT License at https://github.com/mitmedialab/dcpctrl_v1.

Submitted 3 February 2017
Accepted 5 April 2017
Published 26 April 2017
10.1126/scirobotics.aam8986

**Citation:** S. J. Keating, J. C. Leland, L. Cai, N. Oxman, Toward site-specific and self-sufficient robotic fabrication on architectural scales. *Sci. Robot.* **2**, eaam8986 (2017).

Science Robotics

# Toward site-specific and self-sufficient robotic fabrication on architectural scales

Steven J. Keating, Julian C. Leland, Levi Cai, and Neri Oxman

*Sci. Robot.* **2** (5), eaam8986. DOI: 10.1126/scirobotics.aam8986







*Science Robotics* (ISSN 2470-9476) is published by the American Association for the Advancement of Science. 1200 New York Avenue NW, Washington, DC 20005. The title *Science Robotics* is a registered trademark of AAAS.